NANO LETTERS

pubs.acs.org/NanoLett

Ballistic Thermal Conductance of Graphene Ribbons

Enrique Muñoz, Jianxin Lu, and Boris I. Yakobson*

Department of Mechanical Engineering & Materials Science, Department of Chemistry, and the Smalley Institute for Nanoscale Science and Technology, Rice University, Houston, Texas 77005

ABSTRACT An elastic-shell-based theory for calculating the thermal conductance of graphene ribbons of arbitrary width w is presented. The analysis of vibrational modes of a continuum thin plate leads to a general equation for ballistic conductance σ. At low temperature, it yields a power law $\sigma \sim T^{\beta}$, where the exponent β varies with the ribbon width w from $\beta = 1$ for a narrow ribbon ($\sigma \sim T$, as a four-channel quantum wire) to $\beta = {}^3/_2$ ($\sigma \sim wT^{3/2}$) in the limit of wider graphene sheets. The ballistic results can be augmented by the phenomenological value of a phonon mean free path to account for scattering and agree well with the reported experimental observations.

KEYWORDS Thermal transport, graphene, carbon, theory

The ever-increasing demands for heat dissipation in microelectronic circuits, which are approaching a power density of 100 W/cm^2 in hot spots,[1] add to the challenge of sustaining Moore's law.[2] Traditional heat dissipation remedies rely on forced convection through metallic Cu or Al fins, with thermal conductivities on the order of a few hundred W/m K. More efficient cooling solutions rely on novel material structures with superior thermal conductivity. Recent experiments[3,4] suggest graphene as a good candidate, with measured thermal conductivities of 3000−5000 W/m K for layer lengths l of ∼10 μm. This high thermal conductivity surpasses graphite and is in part attributed to the long phonon mean free path λ in carbon nanostructures, exceeding 500 nm in nanotubes[5,6] and graphene sheets.[3] Therefore, it is expected that thermal transport at the nanoscale will be dominated by a ballistic rather than a diffusive mechanism. On the basis of phonon spectra obtained from an atomistic description of graphene, two independent calculations for the ballistic thermal conductance of a graphene sheet have been reported.[7,8] In particular, a low-temperature dependence of $\sim T^{1.5}$ was obtained for an infinite graphene sheet.[7] Here we present analytical expressions for the ballistic thermal conductance of a ribbon of limited width w, approximating its phonon spectra by the vibrational modes of an elastic shell. With a choice of just a few elastic parameters, this provides an accurate description of the long-wavelength acoustic branches. Because phonons obey Bose−Einstein statistics,[9−11] at low T only acoustic modes are populated and hence continuum elasticity provides an accurate description of thermal transport in this regime. At high T, however, the engaged optical phonons add little to the energy flow because of low group velocities and the acoustic modes remain dominant.[9,12] Therefore, a shell model (proven to be efficient in nanoscale mechanics[13]) should also serve as a good approximation of the vibrational spectra with application to transport over a broad temperature range.

For a ribbon, its length l is much greater than its width w, which in turn is larger than the effective thickness t (i.e., $l \gg w > t$). Accordingly, in reciprocal space its vibrations are represented by discrete wave vector values q_w ($\Delta q_w = \pi/w$) in the transverse direction but by the very dense q_l ($\Delta q_l = 2\pi/l$) in the longitudinal direction (continuum q_l corresponds to $l \rightarrow \infty$). The vibrational frequencies for a ribbon are given by dispersion relations (Supporting Information, SI.I)

$$\omega_b = c_b\mathbf{q}^2, \omega_{LA} = c_{LA}q, \omega_{TA} = c_{TA}q, \omega_\tau = c_\tau q_l \qquad (1)$$

for the bending b, longitudinal LA, and transverse TA acoustical and torsion τ polarizations. Here, $c_b^2 \equiv D/\rho$, $c_{LA}^2 \equiv C/\rho(1-\nu^2)$, $c_{TA}^2 \equiv C/2\rho(1+\nu)$, and $c_\tau^2 \equiv 8(1-\nu)/\rho w^2$, with $\mathbf{q} \equiv (q_l, q_w)$ and $q \equiv |\mathbf{q}|$. c_{LA}, c_{TA}, and c_τ represent the usual speeds of sound, and the quadratic dispersion of the bending mode causes its speed of sound to depend explicitly on the wavelength as $\sim c_b|\mathbf{q}|$. We also note that c_τ for the torsion mode vanishes as $\sim {}^1/_w$ in the limit of a wide ribbon ($c_\tau \sim {}^1/_w$ originates simply from the moment of inertia scaling as $\sim tw^3$ and the torsional rigidity is only $\sim t^3 w$). All acoustic branches of the ribbon are fully defined by its surface mass density ρ, the in-plane rigidity C, and the flexural rigidity D. It is instructive to relate C and D further to the elastic parameters of "effective material", the Poisson ratio ν, and Young's modulus Y: $C = Yt$ and $D = Yt^3/12(1-\nu^2)$. An important advantage of the shell model relative to excessively detailed atomistic descriptions is its transferability to other materials. Indeed, eq 1 can be used for any isotropic planar structure (e.g., graphane CH or fluorinated graphene

Received for review: 12/19/2009
Published on Web: 04/19/2010

DOI: 10.1021/nl904206d | *Nano Lett.* **2010,** *10,* 1652–1656

CF) as long as basic elastic properties are known. To apply specifically to graphene ribbon, we use $\rho = m_c N/wl = 0.75$ mg/m^2 (m_c is the mass of the carbon atom and N is the total number of carbon atoms) and the elastic parameters obtained from ab initio calculations,[14] $C = 345$ J/m^2, $D = 1.46$ eV, $\nu = 0.15$, and $t \approx (D/C)^{1/2} = 0.88$ Å. (This thickness correctly describes the physicomechanical behaviors, i.e., stiffness, vibrations, speeds of sound, etc., and is distinct from the volumetric nominal value $s = 3.5$ Å that merely represents van der Waals c-spacing in graphite; their difference has long caused debate in the literature, which is referred to as the Yakobson paradox.[15−17]) We thus obtain for graphene $c_b = 5.6 \times 10^{-7}$ m^2/s, $c_{LA} = 2.17 \times 10^4$ m/s, $c_{TA} = 1.42 \times 10^4$ m/s, and $c_\tau = (1.46 \times 10^{-6}/w)$ m/s.

In counting the vibrational modes, we retain the discrete summation for the width direction ($q_w = j\pi/w$, $j = 0, 1, \ldots, w/a$). The wave vector q_l is treated as a continuum, and its cutoff ($|q_l| \le q_D$) is chosen, in the spirit of the Debye model, to satisfy the correct number of degrees of freedom $3N - 6 \approx 3N$,

$$\sum_{p=\mathrm{TA,LA,b}} \sum_{j=0}^{w/a-1} \frac{l}{2\pi} \int_{-q_D}^{q_D} \mathrm{d}q_l + \frac{l}{2\pi} \int_{-q_D}^{q_D} \mathrm{d}q_l = 3N$$

Here, $p =$ b, TA, LA, that is, the bending and the TA and LA polarizations are included in the first term and the second term corresponds to torsion. Accordingly, the cutoff is

$$q_D = \frac{3\pi n_s}{3/a + 1/w} \tag{2}$$

where $n_s = N/lw = 0.38$ atoms/Å^2 is the surface number density of atoms and a is a primitive cell size so that w/a represents the total number of modes to be included in the width direction. In the limit of a wide ribbon ($w \to \infty$), the cutoff defined by eq 2 becomes size-independent, $q_D = \pi n_s a$, as expected for a 2D sheet. Figure 1 shows for each polarization branch (p) the two lowest modes ($j = 0$, 1 only), according to eq 1. The bending, TA, and LA for $q_w = 0$, π/w, and the single torsion branch are shown as a function of the q_l wavenumber, $|q_l| \le q_D$. As the width w of the ribbon increases, the curves corresponding to various j's get closer together, whereas the speed of sound in the torsion mode decreases as $1/w$. In the limit of a very wide plate $w \to \infty$, the torsion mode disappears, the wavenumber $q_w = j\pi/w$ becomes continuous, and the subbranches merge into three surfaces consisting of a concentric paraboloid (b) and two concentric cones (TA and LA), as the inset shows.

Ballistic heat flux (energy/time) through a ribbon with temperatures $T + (\Delta T/2)$ and $T - (\Delta T/2)$ maintained at its opposite ends and negligible scattering over its length

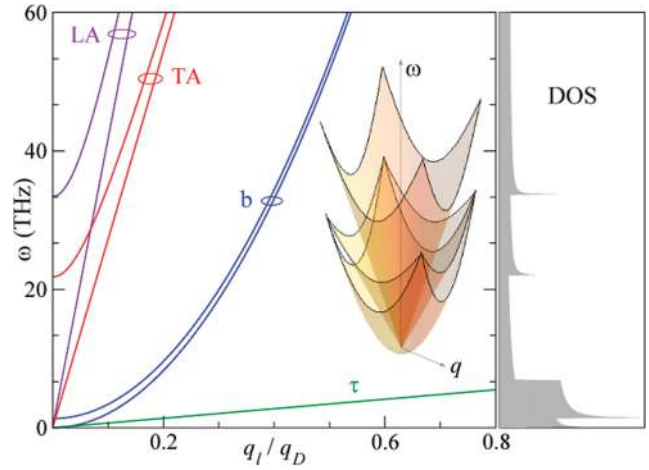

FIGURE 1. Dispersion relations for a narrow ribbon of width $w = 4$ nm obtained from an elastic shell model. The first and second ($j = 0$, 1) lowest branches are displayed for transverse acoustic TA, longitudinal acoustic LA, and bending b, plus a single branch for torsion τ. The right-hand side shows the corresponding density of states (DOS) for these modes together. For a very wide ribbon (infinite 2D-sheet limit, $w \to \infty$), branches $j = 0$, 1, 2,... condense to form a continuum surface for each polarization, as the inset shows.

l can be written as a balance of phonons propagating in opposite directions,

$$\dot{Q} = \int_0^{q_D} \mathrm{d}q_l \sum_{p=\mathrm{TA,LA,b},\tau} {\sum_{j=0}^{w/a-1}}' \frac{1}{2\pi} \hbar\omega_p(\mathbf{q})\, v_{p,l}(\mathbf{q}) \times \left[n\left(\omega_p(\mathbf{q}),\ T + \frac{\Delta T}{2}\right) - n\left(\omega_p(\mathbf{q}),\ T - \frac{\Delta T}{2}\right) \right] \tag{3}$$

Here, $n(\omega, T) = [\exp(\hbar\omega/k_B T) - 1]^{-1}$ is the Bose−Einstein distribution and $v_{p,l} = \partial\omega_j/\partial q_l$ represents the group velocities along the ribbon in the p-th polarization branch. The prime in the Σ' indicates that only branch $j = 0$ should be included for the torsion mode. In defining the thermal conductance along the ribbon as $\sigma = \lim_{\Delta T \to 0} \dot{Q}/\Delta T$, we differentiate $n(\omega, T)$ over T, then integrate explicitly over q_l (while retaining the summation over q_w), and after some algebra obtain

$$\sigma = \frac{{k_B}^2 T}{h} \left\{ \sum_{p=\mathrm{b,LA,TA},\tau} f_2\left(\frac{\theta_p}{T}\right) + \sum_{j=1}^{w/a-1} \left\{ \sum_{p=\mathrm{LA,TA}} \left[f_2\left(\frac{\theta_p \sqrt{1 + (j\pi/q_D w)^2}}{T}\right) - f_2\left(\frac{\theta_p \pi j}{q_D w T}\right) \right] + f_2\left(\frac{\theta_b [1 + (j\pi/q_D w)^2]}{T}\right) - f_2\left(\frac{\theta_b [j\pi/q_D w]^2}{T}\right) \right\} \right\} \tag{4}$$

where $f_n(x) \equiv \int_0^x \mathrm{d}x'\, x'^n e^{x'}/(e^{x'} - 1)^2$. The characteristic temperatures are defined individually for each polarization: $\theta_b = \hbar c_b {q_D}^2/k_B$ and $\theta_p = \hbar c_p q_D/k_B$ for $p =$ LA, TA and τ. Equation 4 is

DOI: 10.1021/nl904206d | Nano Lett. 2010, 10, 1652--1656

rather general and permits either numerical computation or the analysis of different temperatures and ribbon-width limits.

As depicted in Figure 1, the vibrational spectrum has a "gap" separating the four acoustic ($j = 0$) modes $p =$ TA, LA, τ, and b from the higher ones ($j \geq 1$). The size of the gap scales inversely with the ribbon width as $\sim w^{-1}$ for $p =$ LA, TA, and τ but as $\sim w^{-2}$ for $p =$ b. Accordingly, one can define for each polarization the characteristic temperatures $\alpha_b \equiv (\hbar c_b/k_B)w^{-2}$ and $\alpha_p \equiv (\hbar c_p/k_B)w^{-1}$ for $p =$ LA, and TA, above which the first nonacoustic modes become thermally excited according to the Bose−Einstein distribution. Torsion is a single acoustic mode populated at arbitrary low temperatures. In the limit $T \ll \alpha_p$ for all α_p, it can be shown (SI.II) that the asymptotic behavior of the function $f_n(x)$ for $n = 2$ is $f_2(x) \approx (\pi^2/3) + x^2 \exp(-x)$ when $x \gg 1$. By substituting this limit into our general equation 4, we obtain the limit for the thermal conductance at low temperature:

$$\sigma = \frac{4\pi^2 k_B{}^2 T}{3h} + O\left(\left[\frac{\alpha}{T}\right]^2 e^{-\alpha/T}\right) \quad (5)$$

This expression shows that at low temperature the graphene ribbon behaves as a four-channel thermal quantum wire with a thermal conductance $\sim T$. All four channels conduct equally, and each corresponds to one of the acoustic modes, including torsion. We note that this result agrees with the low-T limit of the thermal conductance of a carbon nanotube.[7] For wide ribbons, the spectrum becomes denser, with this effect being more dramatic for the bending mode as reflected in α_b becoming extremely small. Numerically, for a ribbon of 4 nm width the bending characteristic temperature is $\alpha_b \approx 0.3$ K whereas it is as low as 5×10^{-6} K for a micrometer-wide ribbon. In the latter, the four-channel picture is unreachable at any conceivable temperature and the total thermal conductance is proportional to width w.

For the high-temperature limit, we obtain from eq 4

$$\frac{\sigma}{w} = \left(\frac{3}{2}\right) k_B n_s \bar{c} + O(w^{-2}) \quad (6)$$

In this expression, we defined a phase-space average speed of sound for the three acoustic modes, $\bar{c} = [0.65(c_{LA} + c_{TA}) + c_b \pi n_s a]/3$ (details in SI.III). Recall that n_s is the number surface density and that the bending mode has a quadratic dispersion. For graphene, the eq 6 limit in our model is achieved at $T \approx$ 2000 K (on the order of the Debye temperature in graphite).

The graphene sheet case corresponds to a plate of very large width, then $c_\tau \sim {}^1/_w \to 0$ and hence the torsional mode disappears whereas both components of the wave vector $\mathbf{q}$ become quasi-continuous. In eq 4, the discrete sum over j becomes an integral over q_w with density ${}^w/_\pi$ so that the resultant conductance scales as $\sim w$ and should be better defined per unit width as

$$\frac{\sigma}{w} = \sum_{p=b,LA,TA} \int_{q_l>0} \frac{d^2\mathbf{q}}{(2\pi)^2} \hbar\omega_p(\mathbf{q}) v_{p,l}(\mathbf{q}) \frac{\partial n_B(\omega_p, T)}{\partial T} \quad (7)$$

In the high-temperature limit, the thermal conductance is again given by eq 6. Let us now consider the low-temperature limit. As shown in SI.IV, the contribution from the TA and LA modes is $(\sigma/w)_{LA} + (\sigma/w)_{TA} = 0.41(1/c_{LA} + 1/c_{TA})k_B{}^3 T^2/\hbar^2$ whereas the contribution from the bending mode is

$$\frac{\sigma}{w} = \frac{0.23 k_B{}^{5/2} T^{3/2}}{c_b{}^{1/2} \hbar^{3/2}} \quad (8)$$

It is clear that at low temperatures $\sigma \sim T^{1.5}$ for an infinite graphene sheet because of the contribution from the bending mode. This trend agrees with that previously obtained[7] from atomistic calculations, after numerical diagonalization of the dynamic matrices, to obtain the phonon spectra for an infinite graphene sheet. Here, we also see that as the temperature increases, the in-plane LA and TA modes introduce an additional $\sim T^2$ contribution into the thermal conductance.

In Figure 2, to make a fair comparison of ribbons of different widths w (and also to permit comparison with bulk materials), we show the thermal conductance per unit cross section calculated from eq 4. The nominal cross section is ws, with the $s = 3.5$ Å "thickness" based on the interlayer spacing in graphite.[3,4,7] We notice that at low temperature the thermal conductance per unit cross section approximately follows a power law of $\sigma/ws \sim T^\beta$ where the exponent β varies with the ribbon width. For small ribbons, $\beta = 1$ corresponds to the quantum wire behavior, with 4 quanta of thermal conductance as explained above (eq 5); each of the conduction channels of the wire corresponds to one acoustic mode, including torsion. For wider ribbons, the torsion contribution vanishes while the exponent increases toward $\beta = 1.5$ in the infinite graphene sheet, as in eq 8. In the latter case, we showed that exponent $\beta = 1.5$ emerges from the bending mode dominant contribution at low T.

The analysis above does not account for any scattering of phonons as they propagate from the hot end to the cold end unobstructed (cf. eq 3). To apply to more realistic situations, we can introduce an intrinsic (sample-length-independent) mean-free path λ into our ballistic theory in a phenomenological way. Some insight into its role can be gleaned from comparing the thermal conductance calculated by eq 4 with molecular dynamics (MD) simulations. We use a direct method with periodic boundary conditions in the width direction to minimize edge scattering and compute the thermal conductance of graphene ribbons of different lengths l. A strong dependence of the thermal conductivity on the sample length obtained from MD has been reported.[18] Similar data from MD

DOI: 10.1021/nl904206d | Nano Lett. 2010, 10, 1652--1656

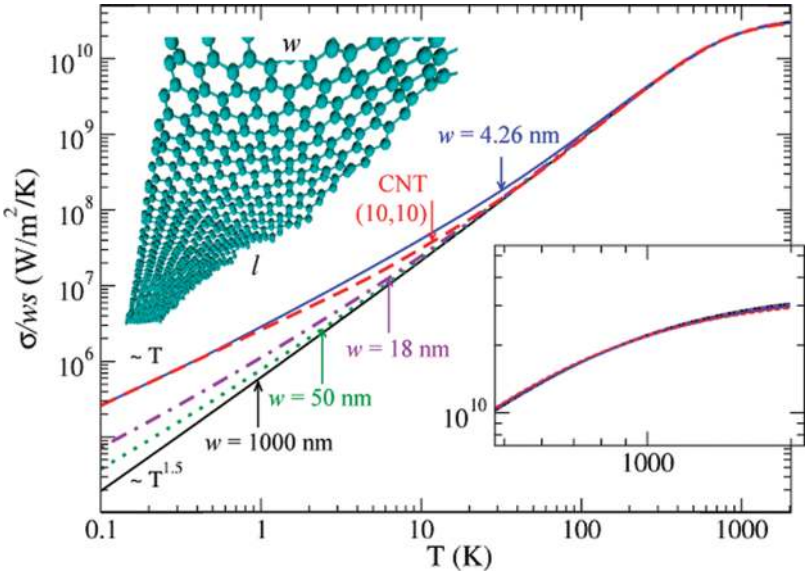

FIGURE 2. Ballistic thermal conductance per unit cross section (σ/ws) as a function of temperature, calculated from eq 4, that does not depend on length l but varies with the width w of the ribbon. The curve becomes independent of width for $w > 500$ nm, reaching the limit of an infinite graphene sheet. Also shown for comparison is our calculated curve for a (10, 10) carbon nanotube.[27] Notice that the narrow graphene ribbon displays the same low-T behavior, $\sim T$, as carbon nanotubes, in agreement with the universal limit in eq 5. Very wide ribbons show a low-temperature dependence of $\sim T^{3/2}$ in agreement with eq 8. The inset shows the high-T behavior.

for carbon nanotubes[19] has been empirically fitted to a dependence $\kappa \sim l^{\alpha}$. This power law is inspired by theoretical results for classical 1D chains, with $\alpha = 1$ corresponding to ballistic transport.[9,20] There is no rigorous justification in extending the results to 2D systems because the effective relaxation times for scattering processes scale differently depending on the dimensionality of the system.[9,21,22] Moreover, in the case of nanotubes the exponent α was not unique but varied with length l.[19] In a different approach, we add the scattering to the ballistic theory through a common heuristic argument. The inverse of conductance, resistivity ($^1/_\kappa$), must be proportional to the frequency of scattering events, with additive contributions from the ribbon ends ($\propto {}^1/_l$) and from intrinsic scattering ($\propto {}^1/_\lambda$), that is, ${}^1/_\kappa \propto {}^1/_l + {}^1/_\lambda$.[9,23] To reproduce the ballistic results correctly in the case of very short samples ($l \ll \lambda$), the general $\kappa(l)$ expression should have the form

$$\kappa(l) = \frac{\left(\frac{\sigma}{sw}\right)l}{1 + \frac{l}{\lambda}} \quad \text{or} \quad \frac{1}{\kappa} = \frac{sw}{\sigma}\frac{1}{l} + \frac{sw}{\sigma\lambda} \qquad (9)$$

Now the data obtained from MD for a series of samples can be used to plot $^1/_\kappa$ as a function of $^1/_l$, as shown in the Figure 3 inset. From the slope and intercept values, one can extract $\lambda_{MD} = 46$ nm, which is low, likely as a result of excessive scattering in MD. Moreover, $(\sigma/sw)_{MD} = 6.7 \times 10^9$ W/m^2 K is close to the results of our ballistic theory, although one should not expect numerical accuracy from the empirical potential-based classical MD model. More essential here is that the data closely follows

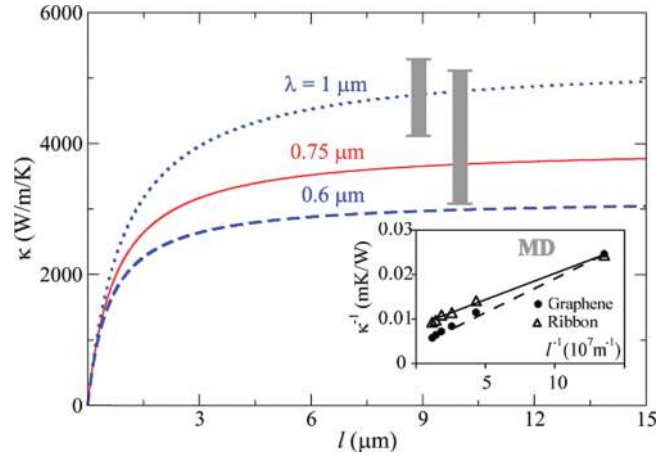

FIGURE 3. Calculated thermal conductivity $\kappa(l)$ for a graphene sheet at room temperature as a function of length, after eq 9. The experiment-based estimate of phonon mean free path $\lambda = 750$ nm,[3] and our theoretical calculation of the ballistic conductance per unit cross section $\sigma/sw = 5.28 \times 10^9$ W/m^2/K at room temperature have been used. For comparison, the curves for $\lambda = 600$ and 1000 nm are also included. The inset shows the data from direct MD simulations ($T = 300$ K, ribbon $w = 2$ nm and graphene) plotted as $^1/_\kappa$ versus $^1/_l$ to support eq 9. Vertical gray bars correspond to the range of values obtained experimentally.[3,4]

the dependence in eq 9 and thus supports the relaxation rates' additivity.[9] One can therefore rely on eq 9, with $^\sigma/_{sw}$ plotted in Figure 2 as computed with our ballistic theory accounting for correct quantum statistics[9−11,24,25] through the Bose−Einstein distribution, and choose λ as one fitting parameter when comparing with experimental measurements.

Before comparing with experimental data, we evaluate the relative contribution from electrons. In graphene, the Fermi surface corresponds just to the K-points in reciprocal space,

DOI: 10.1021/nl904206d | Nano Lett. 2010, 10, 1652--1656

where valence and conduction bands π and π^* do cross. The dispersion in the vicinity of this point, often called the Dirac point, is linear and isotropic,[26] $\varepsilon_{\pm}(\mathbf{q}) - \varepsilon_F = \pm\hbar v_F|\mathbf{q} - \mathbf{q}_F|$. Similar flux considerations as in the case of phonons (eq 3) lead to the electronic part in the ballistic conductance,

$$\frac{\sigma_{el}}{w} = 2\int_{q_l>0}\frac{d^2\mathbf{q}}{(2\pi)^2}(\varepsilon - \varepsilon_F)v_l\frac{\partial n_F}{\partial T} \approx \frac{65k_B{}^3T^2}{h^2v_F} \qquad (10)$$

The latter pertains to the low-temperature limit (details in SI.V), where for common metals electrons usually dominate. Here, however, the electronic contribution at low T is $\sigma_{el}/w \sim T^2$ whereas the phonon contribution is $\sigma_{phon}/w \sim T^{1.5}$, that is, thermal conductance in graphene is in fact dominated by phonons. (This unusual low-temperature dependence has been obtained in ref 8 by a different method.)

We now can compare the predictions of our model with experimental values reported for single graphene sheets in ref 3. This group measured, for graphene sheets with dimensions of $l \approx 10\,\mu$m and $w = 5\,\mu$m, thermal conductivities in the range of 3080−5150 W/m K. They have also estimated the phonon mean free path at room temperature as $\lambda \approx 750$ nm in graphene.[3] In Figure 3, we plot the thermal conductivity as a function of length, predicted from eq 9. (We assume, as in ref 3, that the nominal graphene thickness is $s = 3.5$ Å.) Notice in this plot that eq 9 captures the fact that for $l \ll \lambda$ scattering is negligible and the effective thermal conductivity is proportional to the length l of the sheet whereas the saturation of the curve toward a size-independent, intensive value of the thermal conductivity is achieved for lengths exceeding the average mean free path to a value of $\kappa = 3960$ W/m K according to our theory. The ballistic model, which correctly accounts for the quantum statistics of vibrations and is augmented for scattering by one phenomenological parameter λ, is in good agreement with the reported experimental values of 3080−5150 W/m K at room temperature.[3]

In summary, we presented a theoretical model to estimate the ballistic thermal conductance of a finite-width nanoribbon. It leads to the analytical expressions from a continuum shell model of the ribbon, as an approximation of the acoustic branches in the phonon spectrum, while it preserves the discrete spectrum in the width direction to allow for the treatment of narrow ribbons. At low temperature, our theory predicts a power law for the ballistic thermal conductance of $\sim T^{\beta}$, with a size-dependent exponent that ranges from $\beta = 1$ for narrow ribbons (small w) to $\beta = 1.5$ for a large graphene sheet ($w \to \infty$). In the first limit, we show that the ribbon manifests the conduction properties of a thermal quantum wire with four quanta of thermal conductance, one from each of the acoustic modes: bending, LA, TA, and torsion. Because the speed of sound in the torsion mode is inversely proportional to the ribbon width, in the limit of a very wide graphene sheet the torsion contribution vanishes. For this limit, we show that thermal conduction at low temperature is dominated by the bending mode, with a power law of $\sim T^{1.5}$ (the exponent agrees with numerical calculations previously reported for infinite graphene sheets). The electronic contribution is $\sim T^2$ (at low T) and can generally be neglected, and the pure-phonon predictions of our theory agree well with experimental values ($\kappa =$ 3960 W/m K vs the range of $\kappa = 3080-5150$ W/m K from the experiments with micrometer-sized graphene flakes at room temperature).

Acknowledgment. This work was supported by the Lockheed Martin Corporation, within the LANCER project, and by the Office of Naval Research. We thank Ke Zhao for presenting this work at the American Physical Society March Meeting 2010.

Supporting Information Available. Details of mathematical derivations of the equations presented in the main text. This material is available free of charge via the Internet at http://pubs.acs.org.

REFERENCES AND NOTES

(1) Majumdar, A. *Nat. Nanotechnol.* **2009**, *4*, 214–215.
(2) Lundstrom, M. *Science* **2003**, *299*, 210–211.
(3) Ghosh, S.; Calizo, I.; Teweldebrhan, D.; Pokatilov, E. P.; Nika, D. L.; Balandin, A. A.; Bao, W.; Miao, F.; Lau, C. N. *Appl. Phys. Lett.* **2008**, *92*, 151911.
(4) Balandin, A. A.; Ghosh, S.; Bao, W.; Calizo, I.; Teweldebrhan, D.; Miao, F.; Lau, C. N. *Nano Lett.* **2008**, *8*, 902–907.
(5) Hepplestone, S. P.; Srivastava, G. P. *J. Phys. Conf. Ser.* **2007**, *92*, 012076.
(6) Che, J. W.; Cagin, T.; Goddard, W. A. *Nanotechnology* **2000**, *11*, 65–69.
(7) Mingo, N.; Broido, D. A. *Phys. Rev. Lett.* **2005**, *95*, 096105.
(8) Saito, K.; Nakamura, J.; Natori, A. *Phys. Rev. B* **2007**, *76*, 115409.
(9) Carruthers, P. *Rev. Mod. Phys.* **1961**, *33*, 92–138.
(10) Holland, M. G. *Phys. Rev.* **1963**, *132*, 2461–2471.
(11) Lifshitz, E. M.; Pitaevskii, L. P. *Physical Kinetics*; Butterworth-Heinemann: Oxford, 1997.
(12) Herring, C. *Phys. Rev.* **1954**, *95*, 954–965.
(13) Yakobson, B. I.; Brabec, C. J.; Bernholc, J. *Phys. Rev. Lett.* **1996**, *76*, 2511–2514.
(14) Kudin, K. N.; Scuseria, G. E.; Yakobson, B. I. *Phys. Rev. B* **2001**, *64*, 235406.
(15) Shenderova, O. A.; Zhirnov, V. V.; Brenner, D. W. *Crit. Rev. Solid State Mater. Sci.* **2002**, *27*, 227–356.
(16) Wang, L.; Zheng, Q.; Liu, J. Z.; Jiang, Q. *Phys. Rev. Lett.* **2005**, *95*, 105501.
(17) Huang, Y.; Wu, J.; Hwang, K. C. *Phys. Rev. B* **2006**, *74*, 245413.
(18) Guo, Z. X.; Zhang, D.; Gong, X. G. *Appl. Phys. Lett.* **2009**, *95*, 163103.
(19) Shiomi, J.; Maruyama, S. *Jpn. J. Appl. Phys.* **2008**, *47*, 2005–2009.
(20) Rieder, Z.; Lebowitz, J. L.; Lieb, E. *J. Math. Phys.* **1967**, *8*, 1073–1078.
(21) Livi, R.; Lepri, S. *Nature* **2003**, *421*, 327.
(22) Basile, G.; Delfini, L.; Lepri, S.; Livi, R.; Olla, S.; Politi, A. *Eur. Phys. J.* **2007**, *151*, 85–93.
(23) Datta, S. *Electronic Transport in Mesoscopic Systems*; Cambridge University Press: Cambridge, U.K., 1995.
(24) Klemens, P. G. *Proc. R. Soc. London* **1951**, *208*, 108–133.
(25) Callaway, J. *Phys. Rev.* **1959**, *113*, 1046–1051.
(26) Saito, R.; Dresselhaus, G.; Dresselhaus, M. S. *Physical Properties of Carbon Nanotubes*; Imperial College Press: London, 1998.
(27) Muñoz, E.; Schwarzbart, M.; Yakobson, B. I. Unpublished results, 2009.

DOI: 10.1021/nl904206d | *Nano Lett.* **2010,** *10,* 1652--1656